Communications in Physics, Vol. 31, No. 4 (2021), pp. 389-398
DOI:https://doi.org/10.15625/0868-3166/15843

MAGNETO-ELECTRONIC AND SPIN-POLARIZED TRANSPORT PROPERTIES OF THE ZIGZAG-ZIGZAG PENTA-GRAPHENE NANORIBBON

NGUYEN THANH TIEN†, NGUYEN THANH TUAN AND PHAM THI BICH THAO

College of Natural Sciences, Can Tho University, 3-2 Road, Can Tho City, Vietnam

E-mail: †nttien@ctu.edu.vn

Received 16 January 2021
Accepted for publication 13 June 2021
Published 29 September 2021

Abstract. *Magneto-electronic and spin-polarized transport properties of the zigzag-zigzag penta-graphene nanoribbon are investigated theoretically within the framework of density functional theory combined with non-equilibrium Green's function formalism. It is found that the spin-unpolarized ZZ-PGNR behaves as metal. However, the spin-polarized ZZ-PGNRs show to have the magnetic semiconductor properties. More importantly, for the ZZ-PGNRs based device, the spin-filtering effect occurs strongly near Fermi level. Our findings suggest that ZZ-PGNRs might hold a significant promise for developing spintronic devices.*

Keywords: Electronic; Magnetic; Spin-polarized transport; Zigzag-zigzag penta-graphene nanoribbon.

Classification numbers: 31.15.A, 73.63.-b, 75.75.-c.

I. INTRODUCTION

In 2004, Graphene, a well-known hexagonal two-dimensional material, was discovered by Andre Geim and Konstantin Novoselov. This work was awarded the 2010 Nobel Prize in Physics [1, 2]. Graphene has many attractive physical and chemical properties, and it is of great interest in research [2–5]. The properties of 2D materials can be modified if the building blocks for these nanomaterials are changed from hexagons to pentagons. Following the structure-property

relationships that we have been commonly explored to discover new materials. A carbon allotrope was called penta-graphene (PG), pentagonal arrangement of carbon atoms with the Cairo tiling pattern, was predicted to be a stable configuration [6]. PG has been interested in research recently [7, 8]. PG is a material with a three-layer structure, in which the sp^3 hybrid carbon layer is larded between two layers of sp^2 hybrid carbons. Unlike graphene, PG has a naturally existing band gap. These features hold high promise for developing nanoelectronic devices. Due to unique magneto-electronic properties of the two-dimensional graphene and the corresponding quasi-one-dimensional graphene nanoribbons (GNRs), these materials have been extensively studied for development spintronic devices, using spin instead of charge as an information carrier [9, 10]. Especially one predicts that the zigzag graphene nanoribbons (ZGNRs) will play an important role in spintronic applications [11, 12].

A similar way to graphene, the PG sheets can be cut along typical crystallographic orientations in order to construct various penta-graphene nanoribbons (PGNRs) to obtain quasi-one-dimensional materials. The resulting four types of nanoribbon, with different edge configurations, are denoted as zigzag-zigzag penta-graphene nanoribbon (ZZ-PGNR), zigzag-armchair penta-graphene nanoribbon (ZA-PGNR), armchair-armchair penta-graphene nanoribbon (AA-PGNR), and sawtooth-sawtooth penta-graphene nanoribbon (SS-PGNR). The order of binding energies $E_b(\mathrm{SS}) < E_b(\mathrm{ZZ}) < E_b(\mathrm{ZA}) < E_b(\mathrm{AA})$ suggests greater stability for PGNRs containing more S- or Z-type edges. SS-PGNR has the most stable structure when compared with the other three types of PGNRs with similar width. PGNRs are very versatile, displaying rich and unique electronic and magnetic characteristics [13, 14]. These calculated results showed that SS-PGNR always converges to a spin-unpolarized state (non-magnetic state). SS-PGNR possesses semiconductor properties. Due to the large PG band gap (about 3.25 eV) [6, 15], the current through pure SS-PGNR has small value. Very recently, we have studied the electronic and transport properties of the SS-PGNR in various cases, e.g. the substitutional doping with Si-, N-, P-doped atoms [16], the changing various passivation elements [17], the adsorption of small gas molecules on surface [18] and the uniaxial strain [19]. These research results have shown methods to increase the value of the current through SS-PGNRs.

However, ZZ-PGNR, ZA-PGNR, and AA-PGNR have maintain magnetic states clearly after full convergence, implying that these structures were the magnetic structures. ZZ-PGNR, ZA-PGNR, and AA-PGNR were metallic. Research by Y.H. Li et al. confirmed that ZZ-PGNR, ZA-PGNR, and AA-PGNR can be converted to semiconductors if their edges are passivated by suitable atoms [15]. Bipolar magnetic semiconducting (BMS) features can be achieved in the ferromagnetic state for all magnetic PGNRs, which make PGNRs more valuable [13]. To develop devices based on PGNRs, the spin-polarized transport properties of the magnetic PGNRs should be investigated. In this work, we report first-principles calculations on the magneto-electronic and spin-polarized transport properties of ZZ-PGNR within the framework of density functional theory (DFT) combined with non-equilibrium Green's function (NEGF) formalism. The paper is organized as follows. In Sec. II, the simulation models and computational methods are described. Sec. III demonstrates the results and discussion about the magneto-electronic and spin-polarized transport properties of the studied sample. Finally, Sec. IV presents the conclusions.

II. SIMULATION MODELS AND CALCULATIONAL METHODS

The geometrical optimization as well as calculations for structural stability, magneto-electronic and spin-polarized transport properties are performed by the first-principles method based on the density functional theory (DFT) combined with non-equilibrium Green's function (NEGF) formalism as implemented in the software package Atomistix ToolKit(ATK) [20] (version 2017.4). To solve the Kohn-Sham equation, the Perdew-Burke- Ernzerhof(PBE) formulation of the generalized gradient approximation (GGA) is chosen for exchange correlation potential. Double ζ polarization basis sets are used. The mesh cutoff is chosen as 150 Ry, and a Monkhorst–Pack k-mesh of $1\times1\times12$ is used. The electron temperature (the temperature of the Fermi function) is set to 300 K in our calculations. Structural relaxations were done until residual forces on each atom less than 0.01 eV/Å. Under external bias, the spin-dependent current through the central scattering region can be calculated by Landauer–Büttiker formula [21]

$$I_\sigma(V_b) = \frac{2e}{h}\int_{-\infty}^{\infty} T_\sigma(E,V_b)\,[f(E-\mu_L) - f(E-\mu_R)]\,dE. \tag{1}$$

Here $T_\sigma(E,V_b)$ is the transmission function at energy E under bias V_b in two cases $\sigma =\uparrow$ (spin up) and $\sigma =\downarrow$ (spin down) and can be obtained by the following formula:

$$T_\sigma(E,V_b) = Tr[\Gamma_L(E,V_b)G(E,V_b)\Gamma_R(E,V_b)G^\dagger(E,V_b)]_\sigma, \tag{2}$$

and $f(E-\mu_L)$, $f(E-\mu_R)$ are the Fermi distribution functions for left/right lead electrochemical potentials ($\mu_L = E_f + eV_b/2$, $\mu_R = E_f - eV_b/2$), respectively.

In equation (2), $G^\dagger$ (G) are the retarded (advanced) Green functions and $\Gamma_{L/R}$ are the coupling matrices with the left and right electrodes, respectively.

We consider the ZZ-PGNR with the width of seven carbon chains. Their two edges are terminated by hydrogen non-metallic atoms. A vacuum space of about 20 Å in the lateral directions of the nanoribbon is used to avoid interatomic interactions. This structure is stable in the nonmagnetic state [13].

We evaluate an homogeneous device model with the scattering region is connected to two electrodes which also are magnetic semiconductor.

III. RESULTS AND DISCUSSION

To fully explore the magnetic structure and magnetic distribution in ZZ-PGNR, spin-unpolarized configuration and nine possible magnetic configurations ($\alpha\alpha\alpha$-$\alpha\alpha\alpha$, $\beta\beta\beta$-$\beta\beta\beta$, $\alpha\alpha\alpha$-$\beta\beta\beta$, $\alpha\alpha\alpha$-$\alpha\beta\alpha$, $\alpha\beta\alpha$-$\alpha\alpha\alpha$, $\beta\beta\beta$-$\alpha\beta\alpha$, $\alpha\beta\alpha$-$\beta\beta\beta$, $\alpha\beta\alpha$-$\beta\alpha\beta$, $\alpha\beta\alpha$-$\alpha\alpha\beta$) are initially set as show in Fig. 1. Here, α denote the spin-up component, β denote the spin-down component.

The calculations show that ZZ-PGNR maintain magnetic states clearly after full convergence, implying that these states are solutions of the magnetic structures. For illustrate, Fig. 2 depicts the spin charge density distribution of ZZ-PGNR in nine magnetic configurations. The local magnetic moment is distributed mainly on the specific sp^2-C atoms and is highly localized at two edges. The total energies of the structures after optimization have a negative value as shown in Table 1. This confirms the stability of the research structures. In the evaluated magnetic

configurations, the $\alpha\beta\alpha$-$\alpha\alpha\beta$ configuration is the lowest energy configuration. This configuration should be the basic magnetic configuration. The total magnetic moment per super-cell was calculated using the Mulliken population analysis. In nine studied magnetic configurations, four magnetic configurations ($\alpha\alpha\alpha$-$\alpha\alpha\alpha$, $\beta\beta\beta$-$\beta\beta\beta$, $\beta\beta\beta$-$\alpha\beta\alpha$, $\alpha\beta\alpha$-$\beta\beta\beta$) have significantly large magnetic moment compared to the others. In addition, the magnetic moment of the other magnetic configurations is very small.

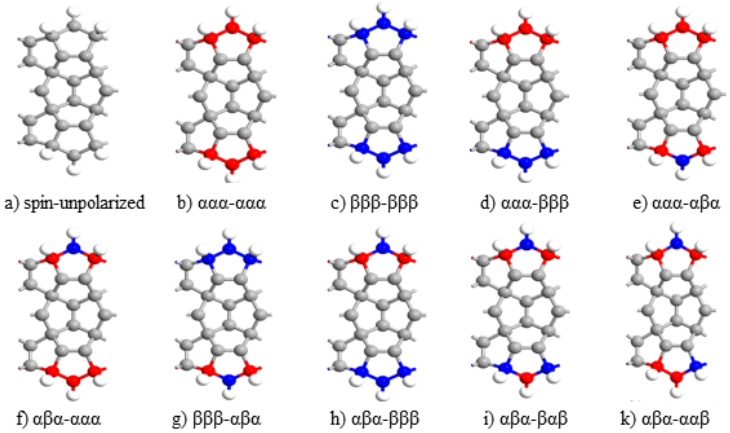

Fig. 1. Schematic of ten different initial configurations based on ZZ-PGNRs: a) spin-unpolarized, b) $\alpha\alpha\alpha$-$\alpha\alpha\alpha$, c) $\beta\beta\beta$-$\beta\beta\beta$, d) $\alpha\alpha\alpha$-$\beta\beta\beta$, e) $\alpha\alpha\alpha$-$\alpha\beta\alpha$, f) $\alpha\beta\alpha$-$\alpha\alpha\alpha$, g) $\beta\beta\beta$-$\alpha\beta\alpha$, h) $\alpha\beta\alpha$-$\beta\beta\beta$, i) $\alpha\beta\alpha$-$\beta\alpha\beta$, k) $\alpha\beta\alpha$-$\alpha\alpha\beta$. Red and blue denote the α- and β- spin components.

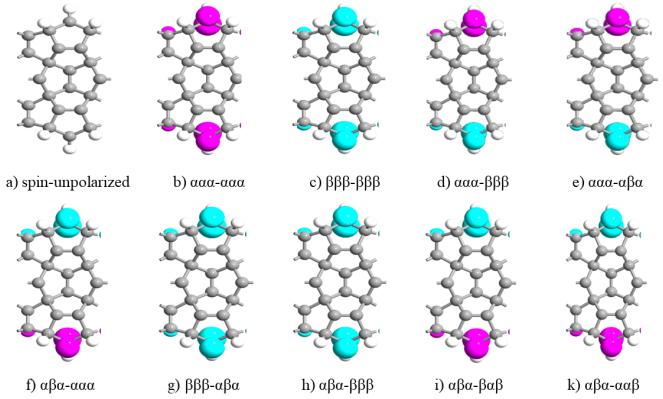

Fig. 2. Schematic of ten different magnetic configurations based on ZZ-PGNRs after the optimized structures: a) spin-unpolarized, b) $\alpha\alpha\alpha$-$\alpha\alpha\alpha$, c) $\beta\beta\beta$-$\beta\beta\beta$, d) $\alpha\alpha\alpha$-$\beta\beta\beta$, e) $\alpha\alpha\alpha$-$\alpha\beta\alpha$, f) $\alpha\beta\alpha$-$\alpha\alpha\alpha$, g) $\beta\beta\beta$-$\alpha\beta\alpha$, h) $\alpha\beta\alpha$-$\beta\beta\beta$, i) $\alpha\beta\alpha$-$\beta\alpha\beta$, k) $\alpha\beta\alpha$-$\alpha\alpha\beta$. Pink and cyan denote the α- and β- spin components. The values for the α- and β- spin isosurfaces are $\pm 0.05\ |e|V/\AA^3$.

Table 1. Total energies and magnetic moments in different magnetic configurations per a super-cell. Here, α denote the spin-up component, β denote the spin-down component.

Magnetic configurations	Total energies (eV)	Magnetic moments (μ_B)
spin-unpolarized	-3679.4578	0.000
$\alpha\alpha\alpha$-$\alpha\alpha\alpha$	-3680.0082	2.002
$\beta\beta\beta$-$\beta\beta\beta$	-3680.0072	-1.998
$\alpha\alpha\alpha$-$\beta\beta\beta$	-3679.9965	0.002
$\alpha\alpha\alpha$-$\alpha\beta\alpha$	-3680.0093	0.002
$\alpha\beta\alpha$-$\alpha\alpha\alpha$	-3680.0099	0.001
$\beta\beta\beta$-$\alpha\beta\alpha$	-3680.0123	-1.999
$\alpha\beta\alpha$-$\beta\beta\beta$	-3680.0117	-2.005
$\alpha\beta\alpha$-$\beta\alpha\beta$	-3680.0092	-0.002
$\alpha\beta\alpha$-$\alpha\alpha\beta$	-3680.0137	0.002

III.1. Magneto-electronic properties

To investigate the magneto-electronic properties of the studied structures, the spin-polarized electronic band structure of magnetic configurations were calculated as shown in Fig. 3. Clearly, the spin-unpolarized ZZ-PGNR behaves as metal. However, the spin-polarized ZZ-PGNRs show to be the magnetic semiconductors. Four magnetic configurations: $\alpha\alpha\alpha$-$\alpha\alpha\alpha$-ZZ-PGNR, $\beta\beta\beta$-$\beta\beta\beta$-ZZ-PGNR, $\beta\beta\beta$-$\alpha\beta\alpha$-ZZ-PGNR, and $\alpha\beta\alpha$-$\beta\beta\beta$-ZZ-PGNR show strong polarization. The energy bands intersecting with the Fermi level in nonmagnetic states split and move upwards or downwards, thus opening a significant band gap adjacent to the Fermi level. Besides, these structures exhibit specific magnetic properties i.e. BMS. ZZ-PGNRs presage richer magneto-electronic properties than ZGNs [22, 23].

The magnitude of the magnetic moment of four BMS configurations are about $2\mu_B$. Both spin-up and spin-down states clearly distinguish. However, only the magnetic moment of ($\alpha\alpha\alpha$-$\alpha\alpha\alpha$) has a positive value. This is favorable for the development of forward spin-polarized transistors. Fig. 4 displays the electronic band structure (BS) and the density of state (DOS) of ZZ-PGNR in ($\alpha\alpha\alpha$-$\alpha\alpha\alpha$) configuration. The energy difference of the two spin channels provides low energy spin-filtering capabilities. This configuration is chosen to investigate spin-polarized electron transport.

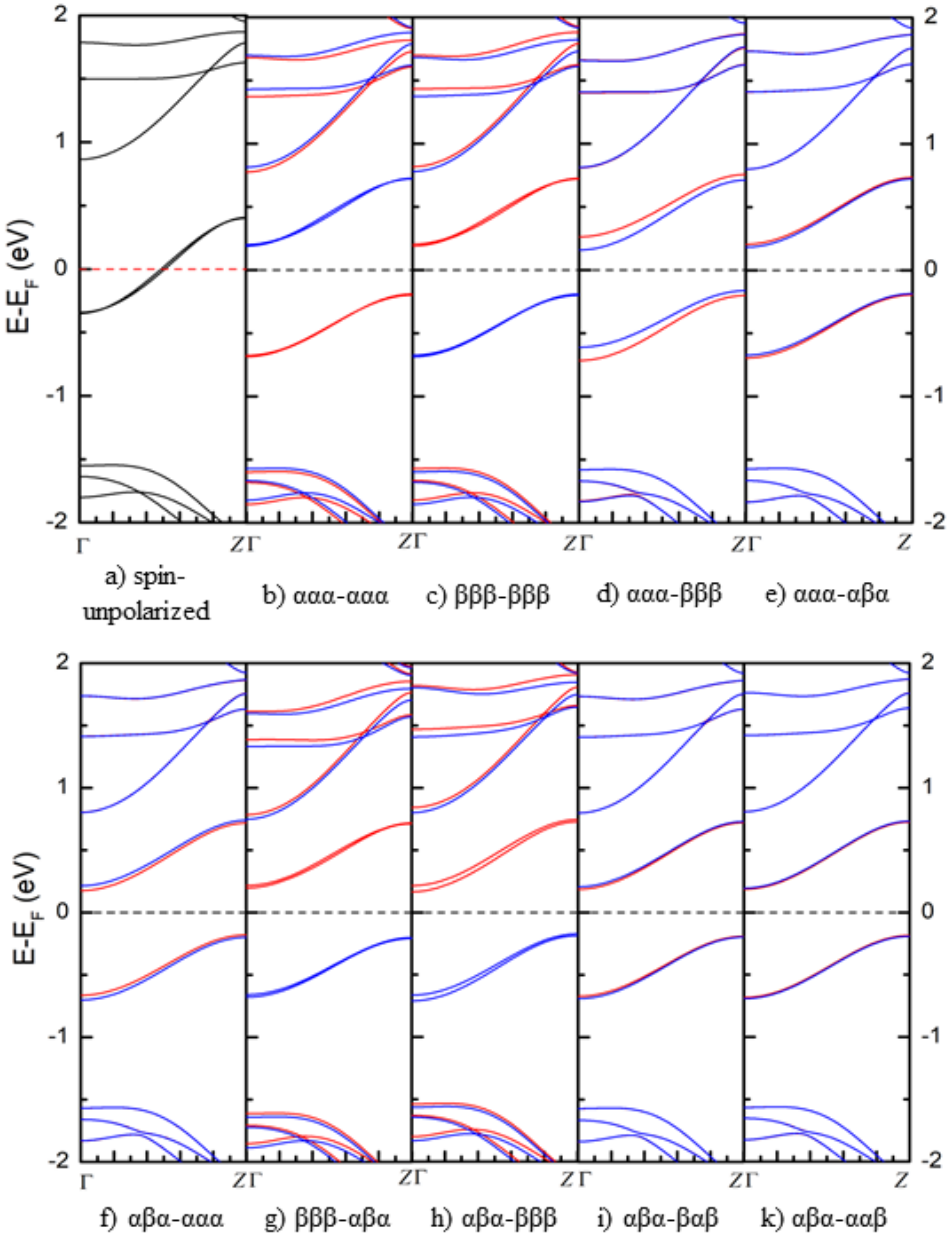

Fig. 3. Band structure of ZZ-PGNRs in different magnetic configurations: a) spin-unpolarized, b) $\alpha\alpha\alpha$-$\alpha\alpha\alpha$, c) $\beta\beta\beta$-$\beta\beta\beta$, d) $\alpha\alpha\alpha$-$\beta\beta\beta$, e) $\alpha\alpha\alpha$-$\alpha\beta\alpha$, f) $\alpha\beta\alpha$-$\alpha\alpha\alpha$, g) $\beta\beta\beta$-$\alpha\beta\alpha$, h) $\alpha\beta\alpha$-$\beta\beta\beta$, i) $\alpha\beta\alpha$-$\beta\alpha\beta$, k) $\alpha\beta\alpha$-$\alpha\alpha\beta$. Red and blue denote the α (up)- and β (down)- spin components.

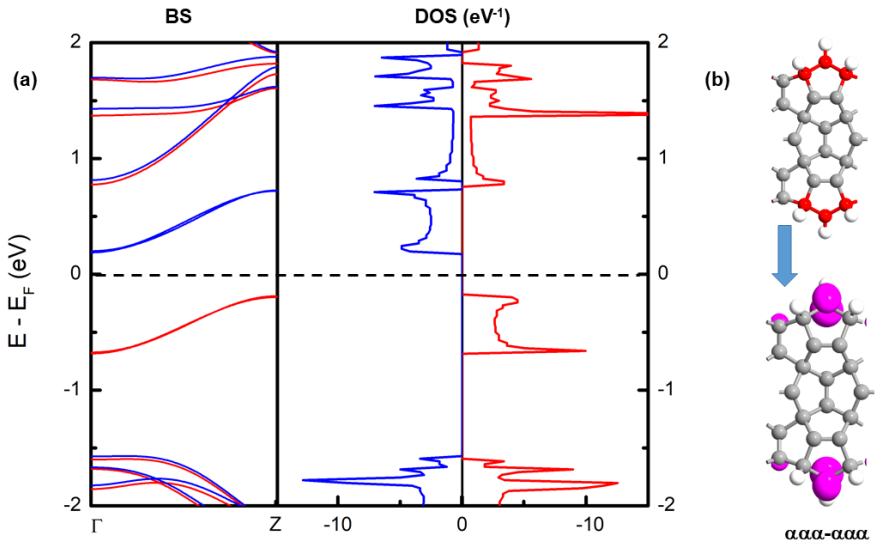

Fig. 4. Magneto-electronics properties of ZZ-PGNR in ($\alpha\alpha\alpha$-$\alpha\alpha\alpha$) magnetic configuration - Left: BS, Center: DOS and Right: Magnetic configuration (The value for the spin isosurfaces is $\pm 0.05\ |e|\,V/\mathring{A}^3$).

III.2. Spin-polarized transport properties

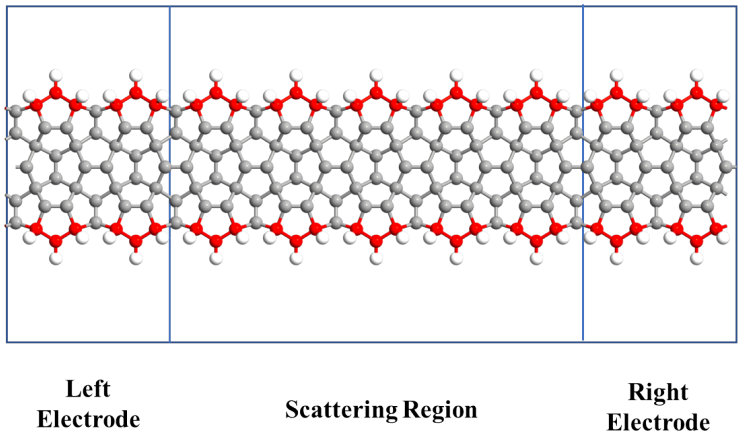

Fig. 5. Schematic structure of the H-terminated ZZ-PGNR device with the width of seven carbon chains. The whole device consists of a central scattering region and two corresponding electrodes

Modeling of ZZ-PGNR device was constructed in Fig. 5 to investigate spin-polarized transport behaviors, where a device is divided into three regions: left electrode, right electrode, and the

scattering region. Each electrode is represented by two unit cells of ZZ-PGNR, and the scattering region is involved by five unit cells of ZZ-PGNR. The spin-unresolved and spin-resolved I-V characteristics are shown in Fig. 6. Obviously, several important features can be visible:

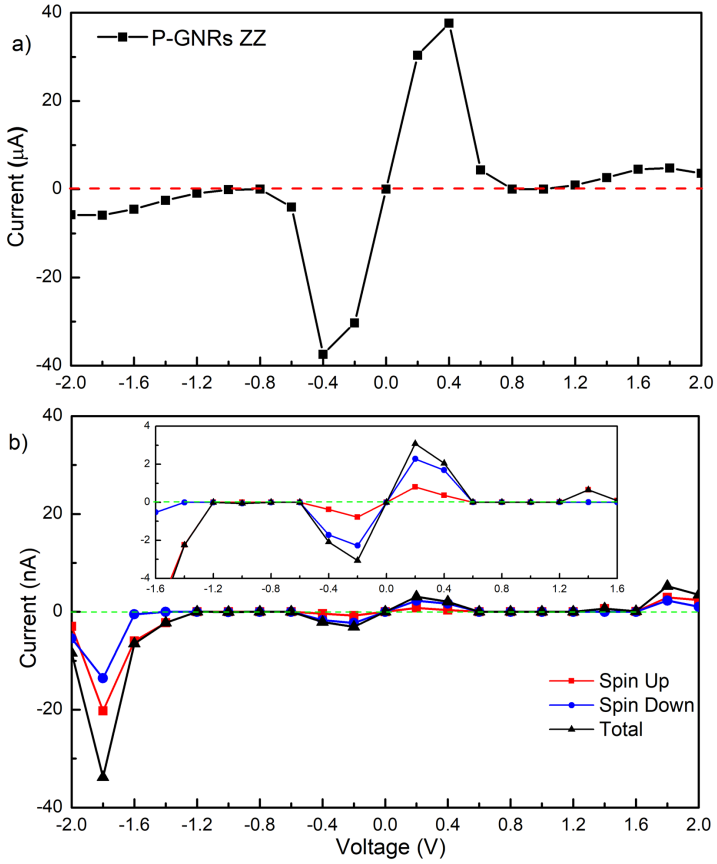

Fig. 6. The I-V characteristics of: a) spin-unresolved ZZ-PGNR and b) spin-resolved ZZ-PGNR in ($\alpha\alpha\alpha$-$\alpha\alpha\alpha$) configuration. The red, blue and black lines denote the spin-up, spin-down and total currents, respectively. The inset in figure b) shows the magnified currents in the bias voltage range from -1.6 V to 1.6 V.

(i) The current of spin-unresolved ZZ-PGNR increases by 3 orders of magnitude compared to that of spin-resolved ZZ-PGNR. This is easily perceived as that the spin-unpolarized ZZ-PGNR show metallic behavior. Otherwise, the spin-polarized ZZ-PGNRs show magnetic-semiconductor behavior (see Fig. 3).
(ii) The electron transmitted channels for both spin-up and spin-down states are almost blocked off completely, in a region from -1.2 to -0.6 V and from 0.6 to 1.2 V. Otherwise, the spin-polarized current is opened under bias: (from -2.0 to - 1.6 V), (from -0.6 to 0.6 V) and (from 1.6 to 2.0 V).
(iii) Tendency of I-V curve is almost symmetrical.
(iv) The spin filter coefficient [24] in (0.2 V and -0.2 V) bias are slightly high: $\mu_{0.2} \sim 43.5\%$, $\mu_{-0.2} \sim 40.2\%$).

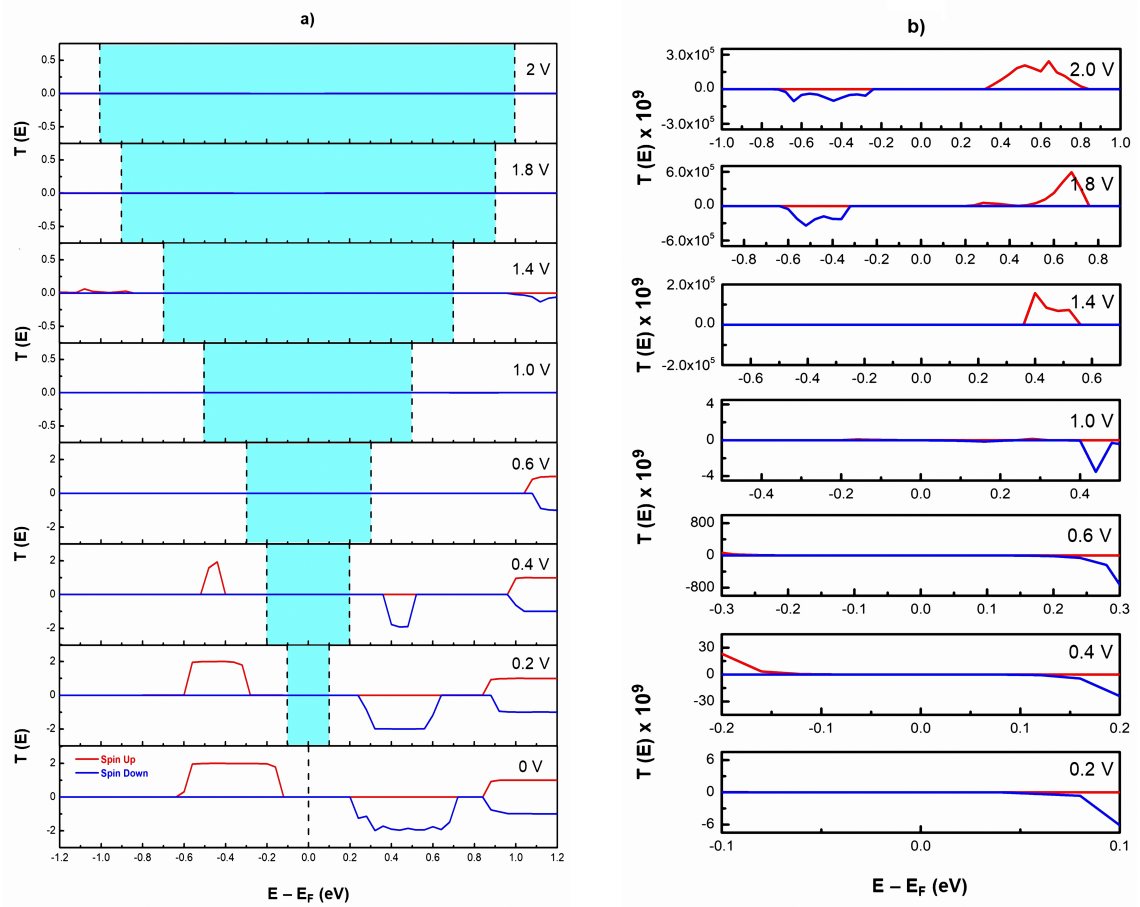

Fig. 7. a) Spin-resolved transmission spectrum T(E) of ($\alpha\alpha\alpha$-$\alpha\alpha\alpha$) magnetic configuration at various bias voltages. b) T(E) in the bias window at the various bias voltages has been magnified. The red and blue lines denote the spin-up and spin-down transmission spectrum, respectively.

To understand the origin of magnetic transport behaviors, the spin-resolved transmission spectrum under several typical biases from 0.0 to 2.0 V is displayed in Fig. 7. The values of T(E) in the bias window are very small (Fig. 7 a)). To illustrate the trend of I-V curves, the bias windows are enlarged in the Fig. 7 b). Because of that, the filled zone bounded by horizontal axis and T(E) curve (in both cases spin-up and spin-down) in bias window help us to explain changing tendency of the I–V curves. These windows with the red and blue lines show the spin-up and spin-down transmission spectrum, respectively. Due to the symmetry of I-V curve, it is sufficient to calculate T(E) spectrum for positive bias voltage domain. As shown in Fig. 7 b), in bias voltage range from 0.0 to 0.6 V, the spin-down transmissions are greater than the spin-up transmission. In bias voltage range from 0.6 to 1.2 V, the spin-up transmissions are always zero. However, in bias voltage range from 1.4 to 2.0 V, the spin-down transmissions are smaller than the spin-up transmissions. Remarkably, these obtained results are entirely consistent with the properties of I-V curves in Fig. 6 [11].

IV. CONCLUSIONS

In summary, the magneto-electronic and spin-polarized transport properties of the ZZ-PGNR have been studied systematically based on a combination of DFT and NEGF formalism. Our calculation results have shown that the spin-polarized ZZ-PGNRs expose the magnetic semiconductor properties. So spin polarization and direction of the current through the device based on ZZ-PGNRs can be controlled through either the source-drain bias voltage or by magnetic configuration of the electrodes. This allows us to theoretically design spin transistors and make it possible to manipulate spin-polarized current for the penta-graphene based nanospintronics. Moreover, BMS materials may be very advantageous for developing next-generation information storage devices. However, the current of these pure spin-polarized ZZ-PGNR structures has a relatively small value ($\sim$ nA). For more realism, a suitable magnetic doping or electrode design is needed to be able to increase the spin-polarized current values.

ACKNOWLEDGMENT

This research is funded by Vietnam National Foundation for Science and Technology Development (NAFOSTED) under grant number 103.01-2020.16. Also, we would like to thank the Information and Network Management Center, Can Tho University for the computational support.

REFERENCES

[1] K. Novoselov, *Rev. Mod. Phys.* **83** (2011) 837.
[2] J. Phiri, P. Gane and T. C. Maloney, *Mater. Sci. Eng. B* **215** (2017) 9.
[3] A. K. Geim, *Sci.* **324** (2009) 1530.
[4] N. T. Tien, B. T. Hoc, N. V. Ut and L. Tuan, *Comm. Phys.* **28** (2018) 201.
[5] N. T. Tien, V. T. Phuc and R. Ahuja, *AIP Adv.* **8** (2018) 085123.
[6] S. Zhang, J. Zhou, Q. Wang, X. Chen, Y. Kawazoe and P. Jena, *Proceedings of the National Academy of Sciences of the United States of America* **112** (2015) .
[7] M. Yagmurcukardes, H. Sahin, J. Kang, E. Torun, F. Peeters and R. Senger, *J. Appl. Phys.* **118** (2015) 104303.
[8] T. Stauber, J. I. Beltrán and J. Schliemann, *Sci. Rep.* **6** (2016) 1.
[9] D. Wang, Z. Zhang, Z. Zhu and B. Liang, *Sci. Rep.* **4** (2014) 7587.
[10] B. Dlubak, M.-B. Martin, C. Deranlot, B. Servet, S. Xavier, R. Mattana, M. Sprinkle, C. Berger, W. A. De Heer, F. Petroff et al., *Nat. Phys.* **8** (2012) 557.
[11] M. Zeng, L. Shen, M. Zhou, C. Zhang, Y. Feng et al., *Phys. Rev. B* **83** (2011) 115427.
[12] J. Zeng, K.-Q. Chen, J. He, X.-J. Zhang and C. Q. Sun, *J. Phys. Chem. C.* **115** (2011) 25072.
[13] P. Yuan, Z. Zhang, Z. Fan and M. Qiu, *Phys. Chem. Chem. Phys.* **19** (2017) 9528.
[14] B. Rajbanshi, S. Sarkar, B. Mandal and P. Sarkar, *Carbon* **100** (2016) 118.
[15] Y. Li, P. Yuan, Z. Fan and Z. Zhang, *Org. Electron.* **59** (2018) 306.
[16] N. T. Tien, P. T. B. Thao, V. T. Phuc and R. Ahuja, *Physica E: Low Dimens.* **114** (2019) 113572.
[17] N. T. Tien, P. T. B. Thao, V. T. Phuc and R. Ahuja, *J. Phys. Chem. Solids.* (2020) 109528.
[18] T. Y. Mi, D. M. Triet and N. T. Tien, *Phys. Open* **2** (2020) 100014.
[19] V. V. On, L. N. Thanh and N. T. Tien, *Philos. Mag.* (2020) 1.
[20] J. Taylor, H. Guo and J. Wang, *Phys. Rev. B* **63** (2001) 245407.
[21] S. Datta, *Electronic transport in mesoscopic systems*, Cambridge university press, 1997.
[22] Z. Hua-Lin, S. Lin and H. Jia-Ning, *Acta. Phys. Sin.* **66** (2017) .
[23] Z. Yu, D. Wang, Z. Zhu and Z. Zhang, *Phys. Chem. Chem. Phys.* **17** (2015) 24020.
[24] D. Zhang, M. Long, X. Zhang, F. Ouyang, M. Li and H. Xu, *J. Appl. Phys.* **117** (2015) 014311.